Vibration control of wind turbine tower-nacelle model with magnetorheological tuned vibration absorber

Paweł Martynowicz

AGH University of Science and Technology, Department of Process Control

Abstract

Wind turbine tower dynamic load is related to the fatigue and reliability of the structure. This paper deals with the problem of tower vibration control using specially designed and built numerical and laboratory model. The regarded wind turbine tower-nacelle model consists of vertically arranged stiff rod (representing the tower), and a stiff body fixed at its top representing nacelle assembly that is equipped with horizontally aligned tuned vibration absorber (TVA) with magnetorheological (MR) damper. To model tower-nacelle dynamics, Comsol Multiphysics finite element method environment was used. For time and frequency domain numerical analyses (including first and second bending modes of vibration) of system with TVA and MR damper models, MATLAB/Simulink environment was used with Comsol Multiphysics tower-nacelle model embedded. Force excitation sources applied horizontally to the nacelle, and to the tower itself were both considered. The MR damper real-time control algorithms, including ground hook control and its modification, sliding mode control, linear and nonlinear (cubic and square root) damping, and adaptive solutions are compared to the open-loop case with various constant MR damper input current values and system without MRTVA (i.e. MRTVA in 'locked' state). Comprehensive numerical analyses results are presented along with Vensys 82 full-scale tower-nacelle model validation. Finally, preliminary results of laboratory tests are included.

Keywords

Wind turbine tower vibration, tuned vibration absorber, MR damper, vibration control, tower-nacelle model

Introduction

Wind turbines are emerging renewable energy extraction solutions nowadays. The wind load (and also sea waves load for the offshore structures) that is varying in time as well as rotation of turbine elements are the major contributors to the structural vibration of tower and blades. Cyclic stress, that tower is subjected to, may lead to the decrease in reliable operation time due to structure fatigue wear (Enevoldsen and Mork, 1996) or even failure accident. Tower vibration arises due to various excitation sources as variable wind conditions, including wind shear, Karman vortices, blade passing effect, rotating elements unbalance, sea waves, ice, etc (Jain, 2011). This vibration is generally lightly damped. Damping ratio for the first two tower bending modes is usually less than or equal to 0.5%, excluding aerodynamic damping (Butt and Ishihara, 2011; Hansen et al., 2012; Matachowski and Martynowicz, 2012). The aeroelastic damping for the first tower longitudinal mode is usually of the order of ten times greater than for the first tower lateral mode (Bak et al., 2012; Hansen et al., 2012). The lateral modes of the tower are excited due to Karman vortices, generator operation, sea waves variable load and rotating machinery unbalance rather than due to direct wind load variation and blade passing effect, as for longitudinal modes. In current project, tower vibration is analysed on the basis of specially developed and built tower-nacelle simulation and laboratory models, in which all turbine components (nacelle, blades, hub, shaft, generator and possibly gearbox) are represented by nacelle concentrated mass and mass moments of inertia.

The main solutions utilised to reduce wind turbines towers' vibration are: collective pitch angle control of the blades (cancellation of 3p excitation arising due to differences in inflow conditions for each of the blades and blade passing effect (p is rotor frequency)) and generator electromagnetic torque control (Jelavić et al., 2007; Namik and Stol, 2011; Shan and Shan, 2012). Passive / semiactive

Corresponding author:
Paweł Martynowicz, AGH University of Science and Technology, Department of Process Control, al. Mickiewicza 30, 30-059 Kraków, Poland.
Email: pmartyn@agh.edu.pl

/ active tuned vibration absorbers (TVAs) (Den Hartog, 1985) are gaining more and more interest in wind turbines applications (Enevoldsen and Mork, 1996; Rotea et al., 2010; Tsouroukdissian et al., 2011; Oh and Ishihara, 2013). TVAs are widely spread structural vibration reduction solutions for slender structures, including towers, high buildings, chimneys, etc. In the standard (passive) approach, TVA is being installed at/close to the top of the structure, and it consists of the additional moving mass, spring and viscous damper, which parameters are tuned to the selected (most often first) mode of structure vibration (Den Hartog, 1985; Łatas and Martynowicz, 2012). Passive TVAs work well at the load conditions characterised with a single frequency to which they are tuned, but can not adapt to wide excitation spectrum (comprising e.g. 3*p* frequency) (Kirkegaard et al., 2002). Moreover, in real world conditions, frequency response of such low-damped structures as wind turbines' towers may exhibit some fluctuations in time (Butt and Ishihara, 2011), thus more advanced TVA approaches consider adaptive stiffness and damping solutions to change/tune TVA operating frequency. Among these solutions, magnetorheological (MR) TVAs are placed (Kirkegaard et al., 2002). MRTVAs are TVAs equipped with MR dampers instead of passive viscous dampers (Koo and Ahmadian, 2007). MR dampers are semiactive actuators characterised with simplicity of construction and minor energy requirements as compared with active systems. They utilise specific properties of MR fluid, which changes its apparent viscosity in the presence of magnetic field. MR dampers are filled with such a fluid and equipped with electrical windings to generate magnetic field, thus they provide a wide range of resistance force, fast response times, low sensitivity to temperature and contamination, and high operational robustness. When MR damper deteriorates, it usually still behaves as a passive shock-absorber (Lord Rheonetic, 2002; Sapiński B and Rosół M, 2008; Sapiński B, 2011; Kciuk and Martynowicz, 2011). As simulations and experiments show, implementation of MR damper in TVA system may lead to further vibration reduction in relation with passive TVA.
Several approaches to the problem of wind turbine tower vibration control with MRTVA are presented. Throughout them, ground hook control and its modification, sliding mode control, linear and nonlinear damping, adaptive control and open-loop solutions with various MR damper input current values are regarded, in comparison with system without TVA (i.e. TVA 'locked' by appropriately high input current fed to MR damper coil). First and second bending mode of vibration are both analysed. Two independent, horizontal, concentrated force excitation sources are considered: the first one (designated by $P(t)$) applied to the nacelle, the second one (designated by $F(t)$) applied to the tower midpoint.

The paper is organised as follows. In the forthcoming section, wind turbine tower-nacelle theoretical and Comsol-Simulink models are introduced. Than, vibration control algorithms are presented and followed by simulations results. Laboratory test rig along with preliminary tests results are presented next. Paper is finished with several conclusions.

Wind turbine tower-nacelle model

Theoretical model

The model to be analysed consists of stiff rod arranged vertically, representing wind-turbine tower, and a stiff body connected rigidly to the top of the rod, representing both nacelle and turbine assemblies. The bottom end of the rod (tower) is fixed to the ground via additional foundation. As the first tower bending mode has dominant modal mass participation (ca. fivefold greater than the next mode), vibration reduction system that comprises spring and MR damper (built in parallel) with an additional stiff body, operating all together as TVA, is located at the top of the tower (at nacelle). The horizontal disturbance load, provided in the laboratory conditions by the dedicated modal shaker, may either be concentrated at the nacelle, or applied to the arbitrary tower section, both locations enable to force tower bending modes of vibration. The MRTVA direction of operation is the same as direction of applied excitation (assuming small bending angles).

Regarded model has to fulfil various constraints, among other adequate dimensions, adequate yield strength and modal masses of the structure, mass of the absorber, all corresponding to the commercially available MR damper characteristics to enable reduction of tower deflection amplitude for the allowable MR damper stroke and force ranges, as well as at least partial dynamic similarity (similarity of motions of tower tips) between real-world wind turbine tower-nacelle system and its

scaled model fulfilled, while respecting limited laboratory space and foundation permissible load (Martynowicz, 2014a; Martynowicz and Szydło, 2014; Snamina et al., 2014). Based on all the assumptions and thorough analyses results, Ti Gr. 5 rod was selected to model wind turbine tower, while Lord Co. RD 1097-1 (Lord Rheonetic, 2002) was utilised as TVA MR damper. The parameters of TVA were tuned for the first bending mode of vibration (Den Hartog, 1985; Łatas and Martynowicz, 2012). The absorber mass m_2 was selected to be 10% of the modal mass of the first bending mode of tower-nacelle model m_1 (i.e. mass ratio was $\mu = m_2/m_1 = 0.1$). Schematic diagram of the system idea is presented in Figure 1 while detailed parameters of the model are collected in the Table 1 below (*Scaled simulation model* column). TVA optimal damping is 129.6 Ns/m. The detailed theoretical calculation analyses comprising Euler Bernoulli beam mathematical model, finite element method (FEM) Comsol Multiphysics model, and dynamic similarity with Vensys 82 baseline case including similarity of lengths (deflections), time (natural frequencies), system damping and forces, are not citied here as are covered thoroughly by previous papers (Łatas and Martynowicz, 2012; Matachowski and Martynowicz, 2012; Snamina and Martynowicz, 2014; Snamina et al., 2014).

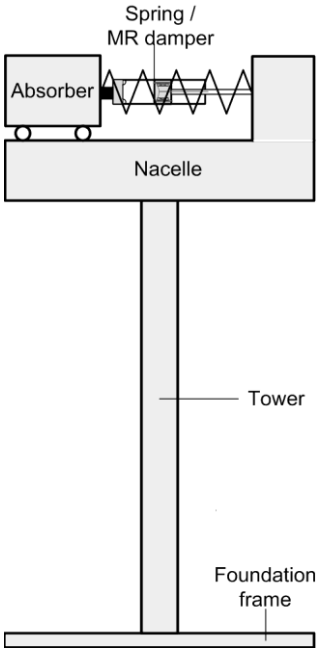

Figure 1. Sketch of the tower-nacelle model with MRTVA.

Comsol-Simulink model

As the idea of current research project was to investigate dynamics of wind turbine tower-nacelle model only together with specially developed vibration reduction system (comprising MRTVA), all turbine components were reduced to mass and mass moments of inertia, while all the aerodynamic loads turbine or tower are subjected to were represented by concentrated forces applied to the nacelle (tower tip) or to the tower section itself. The fundamental emphasis was put on control algorithms design, synthesis and testing as well as laboratory test rig development, thus MATLAB/Simulink software as one of the most appropriate server tools with Comsol Multiphysics environment as FEM client were selected instead of Bladed, FAST, SAMCEF, SIMPACK or other solutions.

Regarding these assumptions, Comsol Multiphysics FEM model of tower-nacelle system was developed and embedded in Simulink environment. The tower-nacelle model was build as a vertical beam fixed at the bottom and free at the top, with an additional mass and mass moments of inertia defined at its top. The model element type of '3D Euler Beam' (smeul3D) with three nodes (points), and 'transient' analysis type were selected (see Figure 2 (a)). Conducted comparative analysis of '3D Euler Beam' with three and seven nodes proved minor influence of additional nodes introduction on analyses results, while very significant influence on computation time. The two edges were configured by applying material properties (Young modulus, Poisson ratio, density, internal friction (Rayleigh damping model), etc.), cross-section dimensions and areas, area moments of inertia and torsional

constant corresponding to the Ti.Gr.5 rod. The bottom node represents tower-ground (tower-foundation) restrain (constraint condition: 'Fixed'), while two other nodes are 'Free'.

Direct or indirect external (aerodynamic, sea waves, ice, etc.) tower loads may be reduced to the resultant concentrated force applied at half of tower height. Thus the node in the tower midpoint (where deflection of the 2nd mode is close to its maximum – see also Figure 2 (c)) is a 'load point' where a horizontal *x*-axis force F ($F(t)$) may be applied. The node at the top of the tower corresponds to the nacelle location, thus mass and mass moments of inertia, as well as concentrated load P ($P(t)$) are all assigned here. The load P acting along *x*-axis represents mainly wind thrust on the tower top / nacelle through the rotor. The node at the top of the tower exhibits maximum deflection of the 1st bending mode (Figure 2 (b)).

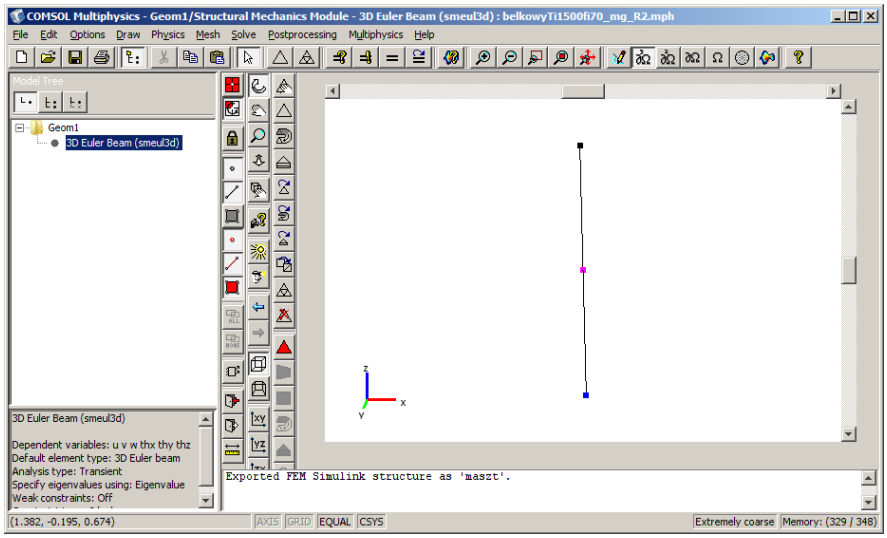

(a)

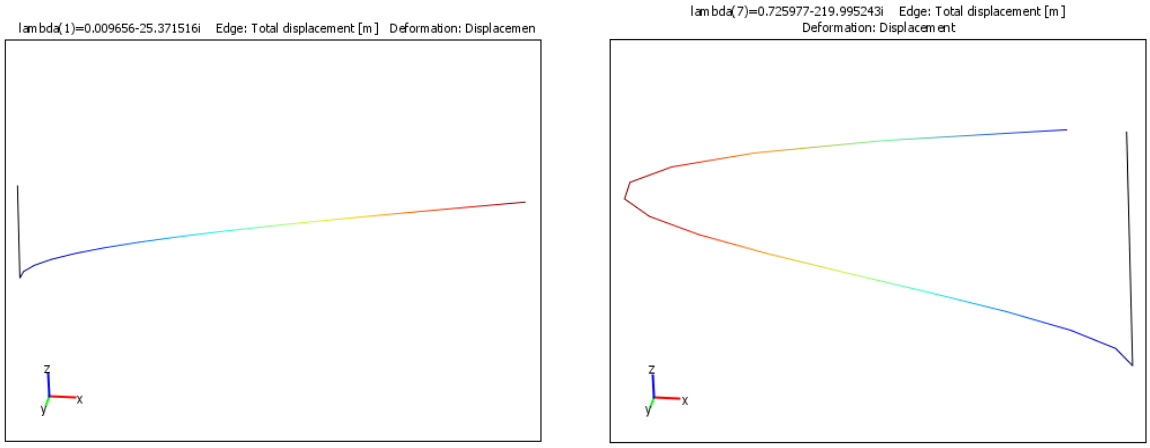

(b) (c)

Figure 2. Comsol Multiphysics tower-nacelle FEM model:
(a) 3D Euler Beam with three nodes, (b) 1st mode shape, (c) 2nd mode shape.

Such a FEM Comsol Multiphysics model was than exported to MATLAB / Simulink. During exporting of *Simulink model*, 'Simulink block type' *General Dynamic* was selected, forces F, P were specified as inputs, while tower tip / nacelle horizontal displacement x_1 and velocity v_1, and tower midpoint displacement x_0 along *x*-axis were defined as three output signals. After exporting, FEM tower-nacelle model was available as MATLAB structure, and Comsol Multiphysics model was embedded in Simulink diagram using *COMSOL Multiphysics Subsystem* block with *Sine Wave* generators P and F as its input signals with amplitudes P_0 and F_0 (respectively), and *To Workspace* blocks as outputs. TVA model acting along *x*-axis was built-in the Simulink diagram. Signals x_1 and v_1

were fed to the dynamics of TVA that was modelled by mass, damping and stiffness parameters m_2, c_2, and k_2 (Den Hartog, 1985; Łatas and Martynowicz, 2012) for the passive case, respectively. By x_2, absorber (TVA mass) horizontal displacement was designated (while v_2 will denote absorber horizontal velocity). If MR damper was used instead of the passive viscous damper, MR damper hyperbolic tangent model (*RD-1097-1 model*) in the form of (Maślanka et al., 2007):

$$P_{MR} = P_c \tanh\{\nu[(\dot{x}_1 - \dot{x}_2) + \mathrm{p}(x_1 - x_2)]\} + c_0[(\dot{x}_1 - \dot{x}_2) + \mathrm{p}(x_1 - x_2)], \tag{1}$$

was embedded in Simulink (Figure 3) instead of *Gain* block modelling c_2. In (1), P_{MR} is the force produced by the MR damper, P_c and c_0 are current-dependent friction force and viscous damping coefficients, ν and p are scaling parameters, while $\dot{x}_1$ and $\dot{x}_2$ are derivatives of x_1 and x_2 with respect to time (respectively). Forces generated by (MR) TVA, acting along *x*-axis at the nacelle (tower tip) were added with appropriate signs to the force *P*. Figure 3 presents Simulink model of such a system with MRTVA.

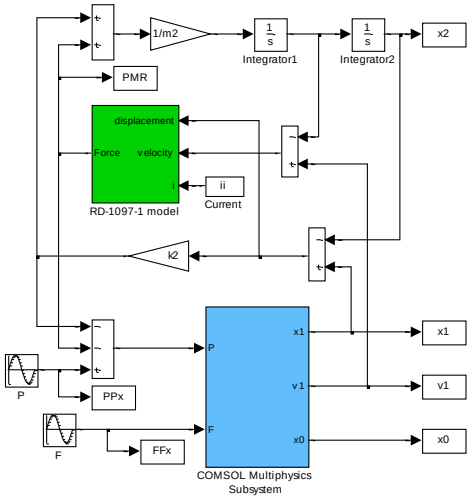

Figure 3. Tower-nacelle FEM model embedded in Simulink.

Control background

Considering nonzero MR damper response time and value of 2nd bending mode frequency (ca. 35 Hz) (Figure 2 (c)), the main purpose of vibration reduction system and TVA implementation was to reduce vibration (namely amplitudes of x_0 and x_1, i.e. A(x_0) and A(x_1)) corresponding to 1st tower-nacelle bending mode only (Figure 2 (b)), thus TVA location was selected to be at the nacelle, where naturally appropriate necessary space may be available in real world conditions. Such a location was also dictated by implementation possibilities of MRTVA at the limited laboratory scale as dimensions of the appropriate MR device are relatively significant.

Equation-set (2) presents model of structure-MRTVA system reduced to 1st bending mode only:

$$\begin{cases} m_1\ddot{x}_1 = -k_1x_1 - c_1\dot{x}_1 - k_2(x_1 - x_2) - P_{MR} + P \\ m_2\ddot{x}_2 = k_2(x_1 - x_2) + P_{MR} \end{cases}, \tag{2}$$

where k_1 and c_1 represent modal stiffness and damping (respectively) corresponding to 1st bending mode of regarded tower-nacelle model, while excitation is applied horizontally to the tower tip (nacelle) thus $P \neq 0$ and $F=0$. Using frequency-domain analysis, assuming that $P=P(t)=P_0\cos(\omega t)$ (ω is angular frequency) and solution is of the form $x_1=x_1(t)=\mathrm{A}(x_1)\cos(\omega t+\varphi)=a\cos(\omega t)+b\sin(\omega t)$, $x_2=x_2(t)=\mathrm{A}(x_2)\cos(\omega t+\psi)=c\cos(\omega t)+d\sin(\omega t)$ (a, b, c, d are real constants), solving for a, b, c, d one may derive values of $\mathrm{A}(x_1)=\sqrt{(a^2+b^2)}$ and $\mathrm{A}(x_2)=\sqrt{(c^2+d^2)}$ amplitudes as a function of excitation frequency.

Analogically, assuming also that $\dot{x}_1 - \dot{x}_2 = \dot{x}_1(t) - \dot{x}_2(t) = A(\dot{x}_1(t) - \dot{x}_2(t))\cos(\omega t + \theta)$, one can obtain: $\varphi=\mathrm{arctg}(-b/a)$, $\psi=\mathrm{arctg}(-d/c)$, $\theta=\mathrm{arctg}[(\sqrt{(a^2+b^2)}\cdot\omega\cos\varphi-\sqrt{(c^2+d^2)}\cdot\omega\cos\psi)/([(-\sqrt{(a^2+b^2)}\cdot\omega\sin\varphi+\sqrt{(c^2+d^2)}\cdot\omega\sin\psi)]$,

with necessary corrections by –π due to periodic nature of tangent function and expected phase characteristics of two degree-of-freedom vibration system elements.

Figure 4(a) presents tower tip displacement amplitude A(x_1) output frequency response functions calculated for excitation amplitude P_0=30.5 N, assuming various P_{MR} functions (see legend, c_2 is damping coefficient of passive TVA tuned according to (Den Hartog, 1985)). Of course in real-world case MR damper force comprises not only viscous, but also friction, and stiffness component. As can be observed, reference characteristics (MR damper producing standard–passive TVA damper force, thick solid black line) exhibits lowest (two) maxima values, equal to $0.96 \cdot 10^{-3}$ m. However, there is a field of further reduction of tower deflection amplitudes by adequate changing of (controlling) MR damper force, namely by increasing damper force in the vicinities of mentioned (two) maxima frequencies (as for thin solid black line), and decreasing damper force in between the frequencies of the two maxima (see dotted line, while grey line characteristics is not practically achievable with the use of MR damper). Figure 4(b) presents phase shift (φ–θ) frequency characteristic for $P_{MR}=c_2(v_1-v_2)=c_2(\dot{x}_1-\dot{x}_2)$. Phase shift between x_1 and $(\dot{x}_1-\dot{x}_2)$ is one of the most frequently utilised and most efficient concepts of TVA control; in this paper *GND* and, indirectly, *Mod.GND* algorithms (described in the next section) outputs are based on signs of x_1 and $(\dot{x}_1-\dot{x}_2)$ functions. When signs of x_1 and $(\dot{x}_1-\dot{x}_2)$ are the same, MR damper force should be maximal, while when signs are opposite, MR damper force should be minimal, according to well known ground-hook principle, as such a control leads to vibration minimisation of the protected structure.

(a)

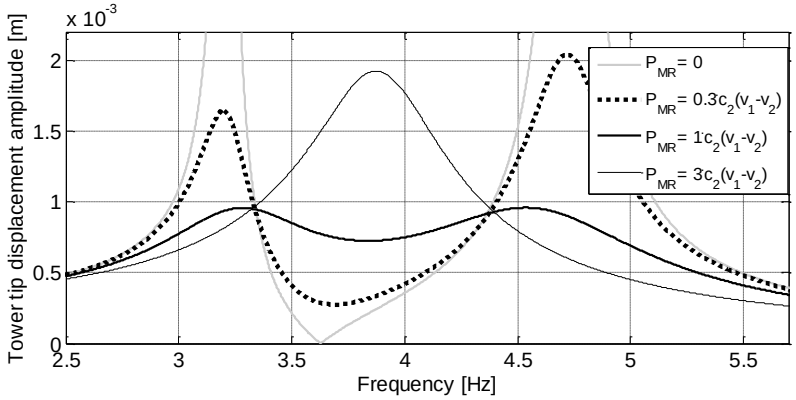

(b)

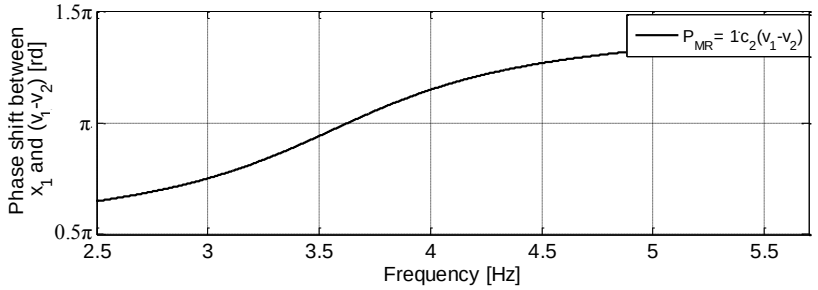

Figure 4. (a) Tower tip displacement amplitude A(x_1) output frequency response functions, (b) Phase shift (φ–θ) frequency characteristic

As can be observed (Figure 4(b)), phase shift (φ–θ) is π at 3.63 Hz (at which A(x_1)=0 for zero damping configuration, see Figure 4(a)). Thus x_1 and $(\dot{x}_1-\dot{x}_2)$ patterns are exactly out-of-phase at 3.63 Hz (where zero damper force is preferable), so equation (4) (and indirectly (5)) yields zero output, i.e. minimum MR damper force. This is also to a large extent the case for all the frequencies between 3.33 Hz and 4.39 Hz, at which two invariant points of amplitude responses appear (Figure 4(a)), resulting small MR damper forces within (3.33, 4.39) Hz range. Outside this range, MR damper forces are maximal in wider intervals, as time intervals in which x_1 and $(\dot{x}_1-\dot{x}_2)$ patterns have the same signs are wider due to the fact that phase shift (φ–θ) noticeably differs from value of π (out-of-phase state).

Details of MR damper control algorithms and their implementation along with simulation analyses and laboratory tests results (validating current section analysis) are presented in the following sections.

Control algorithms

Overview of several approaches to the problem of wind turbine tower-nacelle model vibration control with MRTVA is presented here. With the use of MR damper, standard TVA linear damping algorithm (designated by *C*) (Den Hartog, 1985) may be realised as well as other dedicated solutions. Throughout them, ground hook control (*GND*) and its modification (*Mod.GND*), sliding mode control (*SMC*), nonlinear damping including cubic damping (*C3*) and square root damping (*SQRT*), adaptive MRTVA control (*ADPT*) and open-loop (passive) solutions with 0.0A, 0.1A , 0.2A and 0.3A input MR damper current are regarded, in comparison with system without TVA (i.e. TVA 'locked' by MR damper current of 1.0 A). 1st and 2nd bending mode of vibration are both analysed. As stated above, two independent force excitation sources are considered: one applied horizontally to the nacelle *P* (*P*(*t*)), the other applied to the tower itself at half of its height *F* (*F*(*t*)). As *P*(*t*) is mostly considered to activate the 1st bending mode of vibration, *F*(*t*) is devoted to efficiently stimulate the 2nd mode, however obviously both modes may be activated by either of the excitation sources.

The aim of MRTVA implementation was to reduce tower vibration to even further extend than standard (passive) TVA does. The control strategies that have been employed to determine MR damper current during real-time operation are listed below.

Ground-Hook control (GND)

This strategy was initially developed for vehicle suspension systems (Sapiński, 2008) to minimise tire-road dynamic forces. However implementation of this simple principle for slender structure semi-active TVA / MRTVA is also possible and provides reduction of structure vibration (with relation to the ground) at the point of its application (Shen et al., 2013). The described principle implemented on the MR damper (displacement ground-hook version) is represented by the formula:

$$P_{MR}^{desired} = \begin{cases} P_{MR}^{\max}, & x_1(\dot{x}_1 - \dot{x}_2) \geq 0 \\ 0, & x_1(\dot{x}_1 - \dot{x}_2) < 0 \end{cases}, \text{ thus:} \tag{3}$$

$$i_{MR} = \begin{cases} i_{MR}^{\max}, & x_1(\dot{x}_1 - \dot{x}_2) \geq 0 \\ 0, & x_1(\dot{x}_1 - \dot{x}_2) < 0 \end{cases}, \tag{4}$$

where i_{MR} is MR damper input current. On the basis of thorough simulation analysis, $i_{MR}^{\max}$ = 1.0 A was selected (Martynowicz, 2014b).

Modified Ground-Hook control (Mod.GND)

The original ground-hook modification idea excerpted in this paper arises from the MR damper hysteresis phenomenon. During the sine excitation test, for some part of the period – just after MR damper velocity $(\dot{x}_1 - \dot{x}_2)$ sign change – MR damper behaves as an 'active' device. Although velocity $(\dot{x}_1 - \dot{x}_2)$ sign has already changed, MR damper force sign is maintained for a short part of sine period, thus it may be used for vibration control. This is not the case in TVA system with viscous damper. Basic idea underlying the modified ground-hook algorithm implemented on MR damper takes the form:

$$i_{MR} = \begin{cases} i_{MR}^{\max}, & x_1 P_{MR} \geq 0 \\ 0, & x_1 P_{MR} < 0 \end{cases} \tag{5}$$

where $i_{MR}^{\max}$ = 1.0 A was selected on the basis of simulation series. Details of *Mod.GND* implementation are to be presented in a separate publication.

Sliding mode control (SMC)

Sliding mode control strategy is a nonlinear technique that is widely used due to its robustness and ability to decouple high-dimension systems into a set of independent lower-dimension subsystems

(Neelakantan and Washington, 2008), that is why it was selected for the present system vibration control via MRTVA. Nacelle-TVA dynamics only was regarded here. The sliding surface was selected to be: $s = x_1 + \dot{x}_1$. According to (Neelakantan and Washington, 2008), sliding mode control law may be expressed by equation:

$$P_{MR}^{desired} = \begin{cases} P_{MR}^{\max}, & \text{sign}\left[s\left(\dot{x}_1 - \dot{x}_2\right)\right] = 1 \\ 0, & \text{sign}\left[s\left(\dot{x}_1 - \dot{x}_2\right)\right] \neq 1 \end{cases} \tag{6}$$

thus:

$$i_{MR} = \begin{cases} i_{MR}^{\max}, & \text{sign}\left[s\left(\dot{x}_1 - \dot{x}_2\right)\right] = 1 \\ 0, & \text{sign}\left[s\left(\dot{x}_1 - \dot{x}_2\right)\right] \neq 1 \end{cases} \tag{7}$$

where $i_{MR}^{\max} = 1.0$ A was selected on the basis of simulation series.

Linear damping (C)

In this approach, linear (viscous) damping force is being calculated by simple formula: $P_{MR}^{desired} = c_2\left(\dot{x}_1 - \dot{x}_2\right)$, while internal feedback loop with MR damper real-time force measurement and PI controller is implemented in such a force follow-up control algorithm. PI controller settings are: proportional gain $215 \cdot 10^{-4}$, integral gain $0.2 \cdot 10^{-4}$. Details of implementation of damping force follow-up control algorithm are presented in Figure 5(a) (Laalej et al., 2012) with (0, 1) A saturation limits. An *alpha* is measurement signal scaling factor.

Nonlinear damping (C3 and SQRT)

Previous studies, presented e.g. in (Laalej et al., 2012), confirm beneficial effects of MR damper based implementation of nonlinear damping for vibration control purposes. Two approaches were considered here:

- $P_{MR}^{desired} = K_3 c_2 \left(\dot{x}_1 - \dot{x}_2\right)^3$, i.e. cubic damping, with $K_3 = 50$, $K_3 = 150$ and $K_3 = 250$ selected on the basis of simulation analyses (shortages in graphs: *C3 50*, *C3 150* and *C3 250*, respectively),
- $P_{MR}^{desired} = K_{1/2} c_2 \,\text{sgn}\left(\dot{x}_1 - \dot{x}_2\right)\sqrt{\left|\dot{x}_1 - \dot{x}_2\right|}$, i.e. square-root damping, where $K_{1/2} = 0.25$ and $K_{1/2} = 0.30$ were selected on the basis of simulation series (shortages in graphs: *SQRT 0.25* and *SQRT 0.3*, respectively).

Both approaches comprise damping force follow-up control algorithm mentioned above (see Figure 5(a)).

Adaptive control (ADAPT)

An adaptive solution implemented here is based on using MR damper to emulate controllable (positive and negative) stiffness and controllable viscous damping in such a way that TVA stiffness $k_2^{desired}$ and damping $c_2^{desired}$ is tuned to the excitation frequency rather than to tower-nacelle system 1st bending frequency. Based on this assumption, real-time determination of excitation frequency is followed by real-time calculation of TVA required stiffness P_{stif} and damping P_{damp} forces according to:

$$P_{stiff} = k_2^{desired}\left(x_1 - x_2\right)$$

$$P_{damp} = c_2^{desired}\left(\dot{x}_1 - \dot{x}_2\right) \tag{8}$$

Thus, MR damper required force is:

$$P_{MR}^{desired} = \left(k_2^{desired} - k_2\right)\left(x_1 - x_2\right) + c_2^{desired}\left(\dot{x}_1 - \dot{x}_2\right) \tag{9}$$

where (Den Hartog, 1985; Łatas and Martynowicz, 2012):

$$k_2^{desired} = \frac{\omega_{exc}^2 m_2}{(1+\mu)^2}$$

$$c_2^{desired} = \frac{2\zeta_2 m_2 \omega_{exc}}{1+\mu}$$

$$\zeta_2 = \sqrt{\frac{3\mu}{8(1+\mu)^3}} \tag{10}$$

and ω_{exc} is excitation angular frequency. As MR damper is a semi-active actuator (with a slight exception mentioned in subsection *Modified Ground-Hook control (Mod.GND)*), it cannot deliver energy to the system, thus force (9) cannot be exactly mapped. To cope with this task, force follow-up PI-based control algorithm was specially developed (Figure 5(b)) with (0, 1) A saturation range. PI controller settings were: proportional gain $2{\cdot}215{\cdot}10^{-4}$, integral gain $0.2{\cdot}10^{-4}$.

(a)

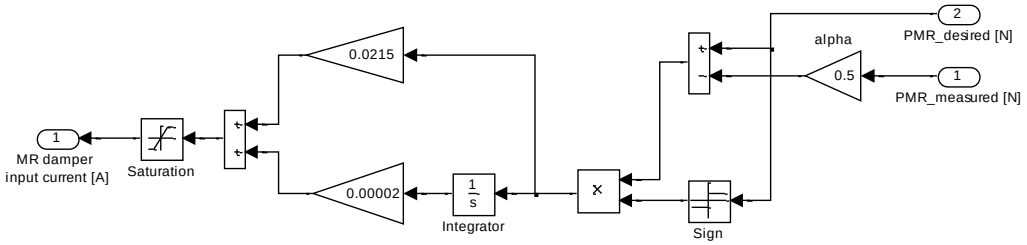

(b)

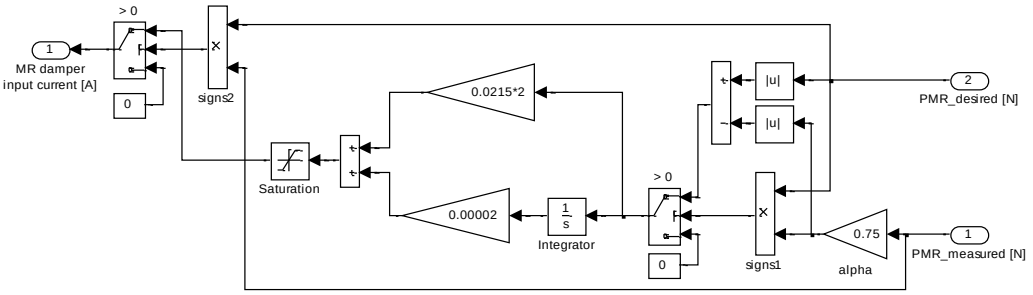

Figure 5. Damper force follow-up control algorithms (Simulink implementations).

Simulation analyses

To determine amplitude of x_0 and x_1 output frequency response functions (A(x_0), A(x_1) respectively), series of simulation analyses were conducted at selected discrete sine excitation frequency points within the range of (3, 40) Hz, comprising 1st and 2nd bending natural frequencies of the system without MRTVA. These natural frequencies, given by Comsol Multiphysics Postprocessor (Figures 2 (b)(c)), are respectively: f_I = 4.04 Hz and f_{II} = 35.01 Hz. Two excitation configurations were investigated during simulations, the first: P_0=30.5 N and F_0=0 N, and the second: P_0=0 N and F_0=305N (information on forces with zero values will be omitted in further descriptions).

Figures 6 (a)(b) show comparison of A(x_0) and A(x_1) output frequency response functions for the system without MRTVA (MRTVA in 'locked' state) and P_0=30.5 N (first excitation configuration) or F_0=305 N (second excitation configuration) sine excitation amplitudes, respectively. For the second excitation configuration, A(x_0) reaches $6{\cdot}10^{-3}$ m at f_{II} (while only $1{\cdot}10^{-4}$ m for the first configuration).

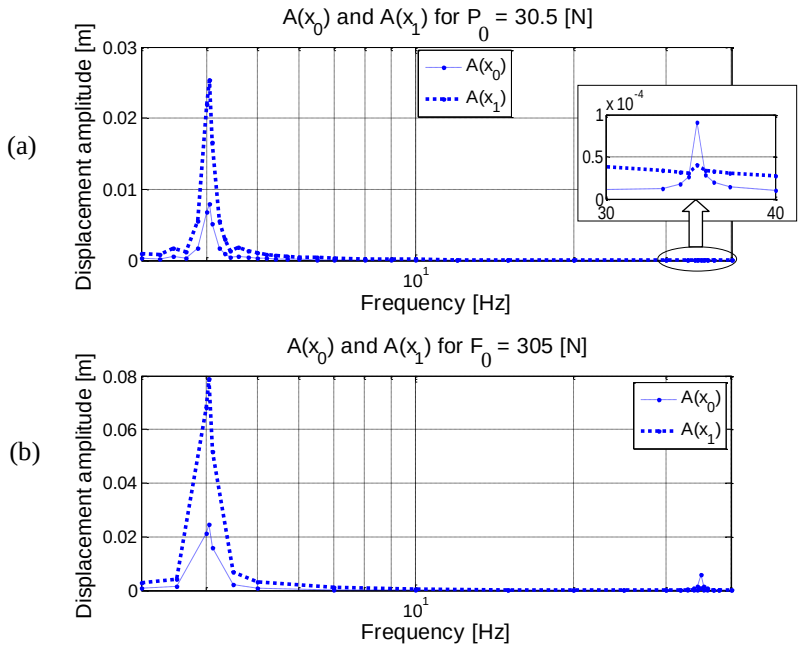

Figure 6. Tower midpoint displacement amplitude A(x_0) and tower tip displacement amplitude A(x_1) output frequency response functions for the system without MRTVA.

Characteristics shown in the Figures 7–10 were obtained for the system with MRTVA. Figures 7 (a)(b)(c) present A(x_0) output frequency response functions determined for open-loop system with constant MR damper input currents (Figure 7(a)), and for feedback system with linear damping, sliding mode control, standard and modified displacement ground-hook, and adaptive control algorithms (Figure 7(b)) as well as nonlinear damping feedback solutions (Figure 7(c)) for the first excitation configuration. Analogically, Figures 8 (a)(b)(c) present A(x_1) output frequency response functions for the first excitation configuration. Figures 9 (a)(b)(c) and Figures 10 (a)(b)(c) show respective frequency response functions determined for the second excitation configuration: A(x_0) (Figures 9) and A(x_1) (Figures 10).

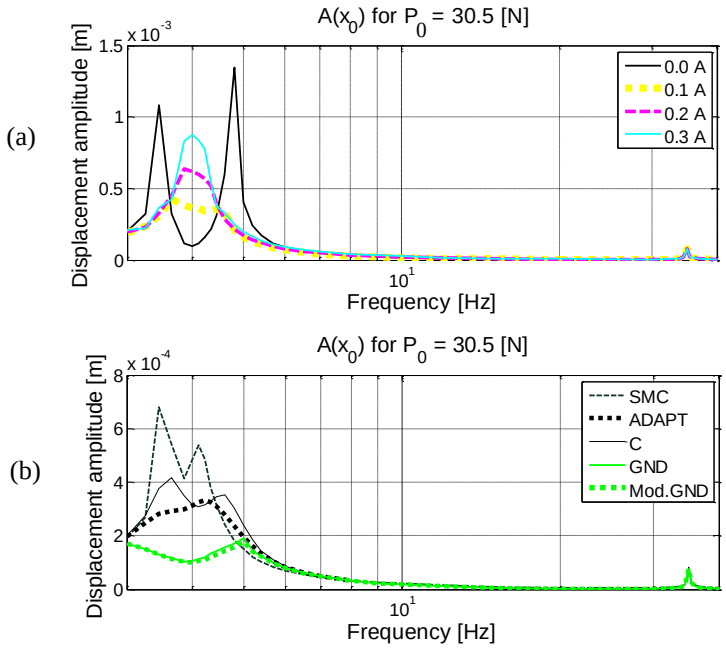

(c)

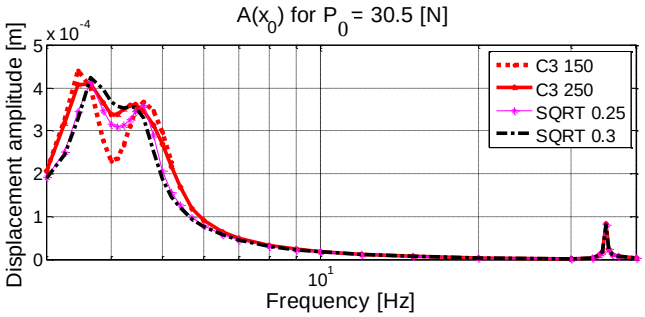

Figure 7. Tower midpoint displacement amplitude A(x_0) output frequency response functions for the system with MRTVA, P_0 = 30.5 N.

(a)

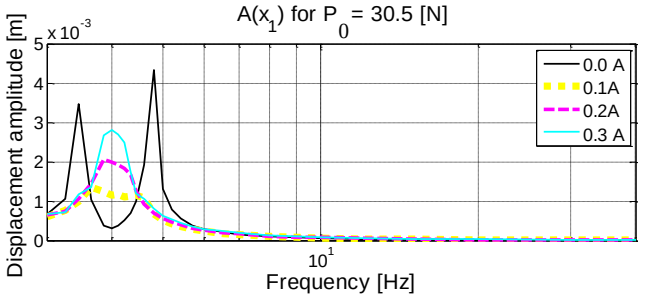

(b)

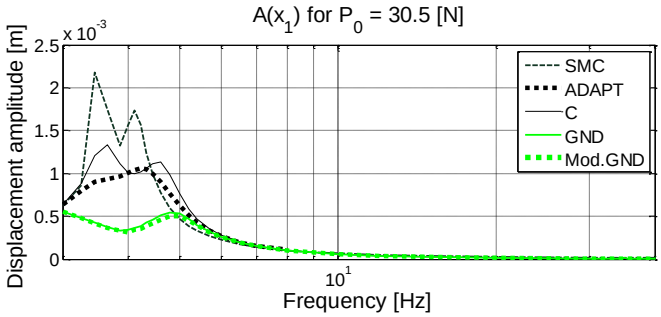

(c)

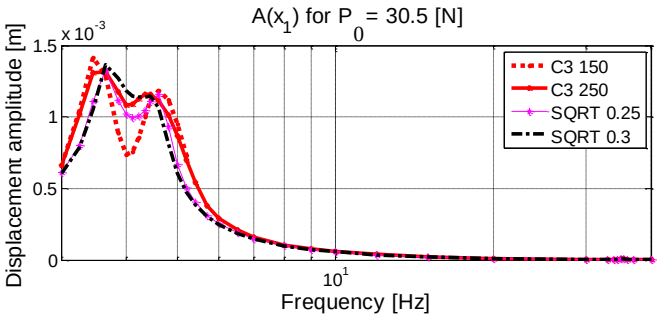

Figure 8. Tower tip displacement amplitude A(x_1) output frequency response functions for the system with MRTVA, P_0 = 30.5 N.

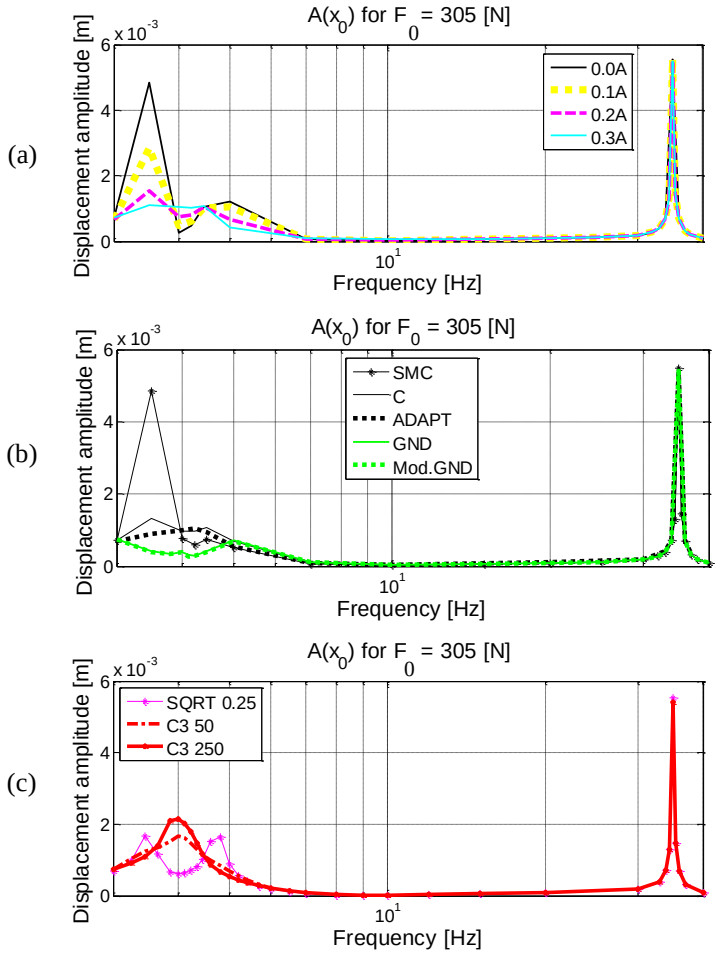

Figure 9. Tower midpoint displacement amplitude A(x_0) output frequency response functions for the system with MRTVA, F_0 = 305 N

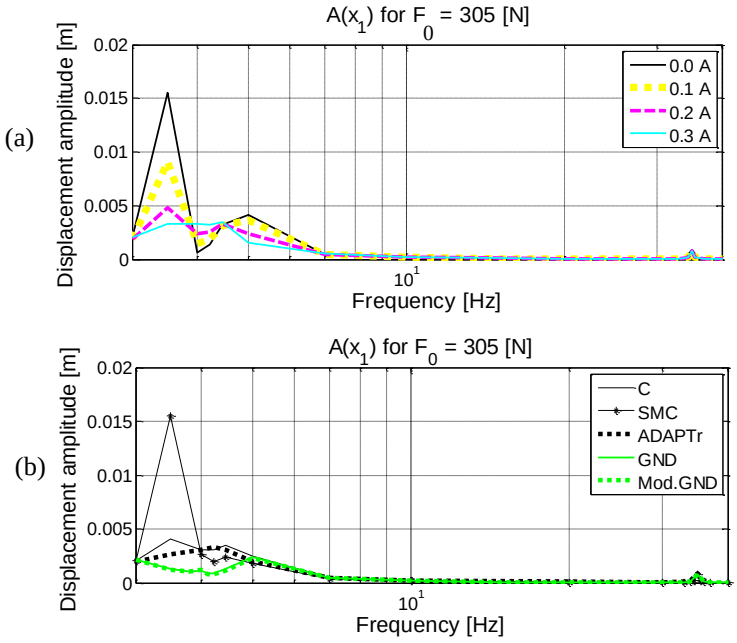

(c)

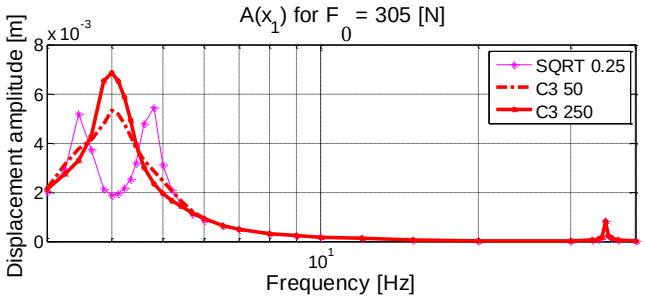

Figure 10. Tower tip displacement amplitude A(x_1) output frequency response functions for the system with MRTVA, F_0 = 305 N.

The presented results prove the potential of MRTVA in tower-nacelle system vibration reduction at frequency of the 1st bending mode, without deterioration at other frequencies. Substitution of passive TVA with MRTVA enables further vibration reduction by application of dedicated control solutions. Maximum amplitudes obtained with *GND* and *Mod.GDN* control algorithms were in the majority of simulation scenarios lesser than half of the maximum amplitudes of the system emulating linear damping as in standard TVA with passive viscous damper (designated by *C*). The accuracy of passive damper force follow-up is limited by the actuator nature. The advantage of *Mod.GDN* algorithm over *GND* may be observed e.g. at frequency of 5.0 Hz (Figure 7 and Figure 8). MR damper current control operation is demonstrated by P_{MR} force values switches reflecting control current impulses between 0 and $i_{MR}^{\max}$ .Time plots presented in Figures 11 and 12 prove that equation (5) produces more favourable MR damper control pattern (observed as x_1 amplitude reduction) than equation (4), due to hysteresis phenomenon of MR damper force-velocity characteristics. *Mod.GDN* algorithm implemented on the experimental ground in comparison with *GND* algorithm is presented as a separate publication (Martynowicz, 2015).

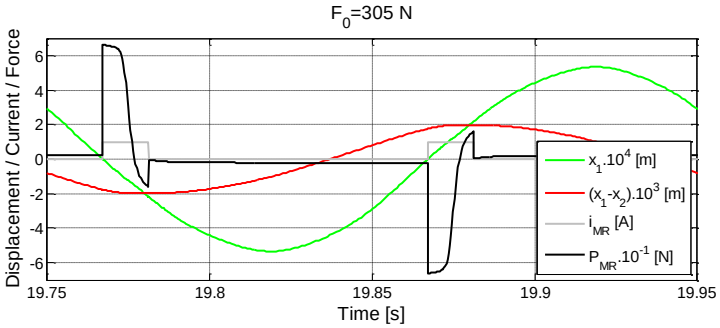

Figure 11. Tower tip displacement x_1, MR damper travel x_1–x_2, current i_{MR} and force P_{MR} for the feedback system with *GND* algorithm, F_0 = 305 N.

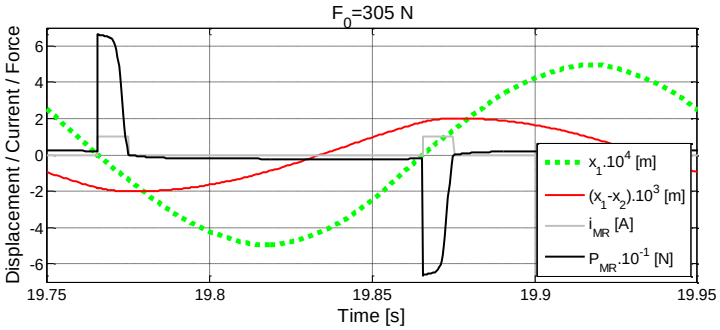

Figure 12. Tower tip displacement x_1, MR damper travel x_1–x_2, current i_{MR} and force P_{MR} for the feedback system with *Mod.GND* algorithm, F_0 = 305 N.

As depicted above, effectiveness of the adaptive control was limited by MR damper semi-active type of actuation and its force variation range, precluding MRTVA possibility to adapt to 2nd bending mode (even neglecting MR damper response time), while benefits of *ADAPT* over standard TVA (i.e. linear

damping, *C*) are noticeable. The *ADAPT* results are quite on par with most favourable open-loop system (*0.1 A*) results for P_0 (tower tip) excitation (Figures 7–8). However for F_0 (tower midpoint) excitation of the 1st mode (Figures 9–10), *ADAPT* copes better than *0.1 A* open-loop system, and comparable to *0.3 A* open-loop (which in turn delivers less favourable characteristics than *ADAPT* for P_0 excitation). Consequently, *ADAPT* algorithm presents better performance than *0.2 A* and *0.0 A* open-loop systems in all conditions considered. Further analyses of *ADAPT* for system parameters uncertainty may be planned in the future. The sliding mode and nonlinear damping control solutions deliver no apparent advantage over MRTVA emulating viscous damping *C*. Further analyses are considered. It was also determined that for laboratory model 2nd bending mode, amplitude $A(x_1)$ is relatively small ($A(x_1) << A(x_0)$) (see Figure 2 (c), Figures 6 – 10) as mass of the nacelle is much higher than tower mass. Moreover, regarding MR damper response time and value of 2nd bending mode frequency, vibration reduction possibilities of MRTVA is very much limited to the 1st bending mode. However, in real-world applications, nacelle displacement amplitude is meaningful for 2nd bending mode while its frequency is below 5 Hz, thus vibration reduction possibilities of MRTVA located at the nacelle are there.

It is worth to point out that Comsol/Simulink co-simulation analyses give the possibilities of testing various MR damper control algorithms for the continuous-discrete system modelled in FEM environment, however computational load is very significant and time consuming.

Validation analyses

The results obtained in the previous section serve as a basis for validation analyses of the regarded model vs. full-scale Vensys 82 wind turbine tower-nacelle baseline structure, assuming nacelle and turbine to be a one solid body (excluding blades aerodynamics). It was previously proven (Snamina and Martynowicz, 2014; Snamina et al., 2014) that conditions of partial dynamic similarity (similarity of motion of tower tips) between regarded model and full-scale structure are fulfilled. Now these former results are verified using FEM model of Vensys 82 tower-nacelle structure embedded (similarly as presented above) in Simulink environment with MRTVA model and dedicated control algorithm. For these analyses, *Mod.GND* algorithm was chosen and compared with reference structure without MRTVA. Vensys 82 tower-nacelle structure FEM model was built as 9-segment non-prismatic beam (a tower) with a solid body mass and mass moments of inertia as a nacelle/turbine. Additionally, modified configuration is proposed with tower mass/stiffness reduced by the factor of two, thanks to the load mitigation by utilisation of MRTVA along with proper vibration control algorithm. The proposed modified tower structure is of the same height and external diameter vertical profile as original structure, however wall thickness is ca. half of the original one. Table 1 presents assumed parameters of the full-scale structure vs. its scaled model, and proposed modified structure, as well as maximum bending stress, maximum deflection and maximum acceleration values corresponding to 1st bending mode of vibration neighbourhood. Comparison of the configuration with and without MRTVA is presented for sine horizontal excitation applied to the nacelle (*P*) for each structure model (for modified Vensys 82 model, variant without MRTVA cannot be considered due to large bending stress values). For both original and modified Vensys 82 models with MRTVA, MR damper force is assumed according to the conclusion of dynamic similarity analysis (see Snamina and Martynowicz, 2014). Regarding real-world turbine aerodynamic damping, preferable TVA operation direction should lie within the plane parallel to the rotor plane. Figures 13 and 14 present tower tip (nacelle) displacement and acceleration amplitude output frequency response functions for baseline and modified Vensys 82 models with MRTVA and *Mod.GND* algorithm, assuming $P_0 = 2.5 \cdot 10^3$ N.

As can be observed in Figures 14, implementation of $6.5 \cdot 10^3$ kg absorber with appropriate spring and MR damper selection along with real-time measurement and control system may lead to both structure overall mass decrease by $78 \cdot 10^3$ kg (or more, up to $84.5 \cdot 10^3$ kg, assuming that some nacelle equipment/frame mass may operate in motion – as absorber mass), and significant bending loads, deflections, and accelerations decrease in comparison with baseline Vensys 82 structure without MRTVA. In case of measurement / control / MR damper failure, internal system watchdog should execute a switch to a passive regime with zero MR damper current that still provides satisfactory properties – in fact some further MR damper force amplitude / *Mod.GND* control system tuning

possibilities (leading to further deflections decrease for *Mod.GND* system) may be inferred from *Mod.GND* and *0.0 A* curves observation. To eliminate (marginally small) risk of MR damper / TVA lock-up failure, it may be considered the implementation of both multi-MR-damper TVA system (MR damper redundancy) and additional passive TVA system with significantly lower absorber mass m_2 that is normally-locked (TVA redundancy); ultimate solution would be particular turbine switch off / cut-out within ca. 500 seconds (depending on tower steel properties) of resonant vibration, when bending stress value for modified Vensys 82 structure is expected to be similar as maximum bending stress for baseline Vensys 82 with no TVA, according to Comsol/Simulink analysis with $P_0 = 2.5 \cdot 10^3$ N.

Table 1. Assumed models parameters and numerical results validation (1st bending mode neighbourhood).

Parameter \ Model / TVA	Scaled simulation model		Baseline Vensys 82 model		Modified Vensys 82 model	
	no TVA	**MRTVA**	**no TVA**	**MRTVA**	**no TVA**	**MRTVA**
Tower type	Prismatic rod		Non-prismatic tube		Non-prismatic tube	
Tower mass [kg]	25.6		$169.0 \cdot 10^3$		$84.5 \cdot 10^3$	
Tower external diameter [m]	0.07		4.52 to 3.30		4.52 to 3.30	
Tower height [m]	1.5		85.0		85.0	
Mass of the assembly located at the top (nacelle w/o absorber) [kg]	166.2	150.6	$90.4 \cdot 10^3$	$77.4 \cdot 10^3$	$90.4 \cdot 10^3$	$83.9 \cdot 10^3$
Absorber mass [kg]	–	15.6	–	$13.0 \cdot 10^3$	–	$6.5 \cdot 10^3$
Mass ratio μ [%]	–	10.0	–	12.6	–	6.7
TVA spring stiffness [N/m]	–	$9.52 \cdot 10^3$	–	$55.97 \cdot 10^3$	–	$16.33 \cdot 10^3$
Amplitude of horizontal load (P_0) [N]	30.5		$2.5 \cdot 10^3$		$2.5 \cdot 10^3$	
Results						
Maximum displacement [m] (top end of the tower / nacelle)	0.079	$0.55 \cdot 10^{-3}$	3.06	0.048	7.98	0.134
Maximum acceleration [m/s^2] (top end of the tower / nacelle)	50.9	0.490	15.0	0.263	22.8	0.331
Maximum bending stress [Pa] (bottom end of the tower)	$406 \cdot 10^6$	$2.82 \cdot 10^6$	$397 \cdot 10^6$	$6.88 \cdot 10^6$	$1130 \cdot 10^6$	$19.0 \cdot 10^6$

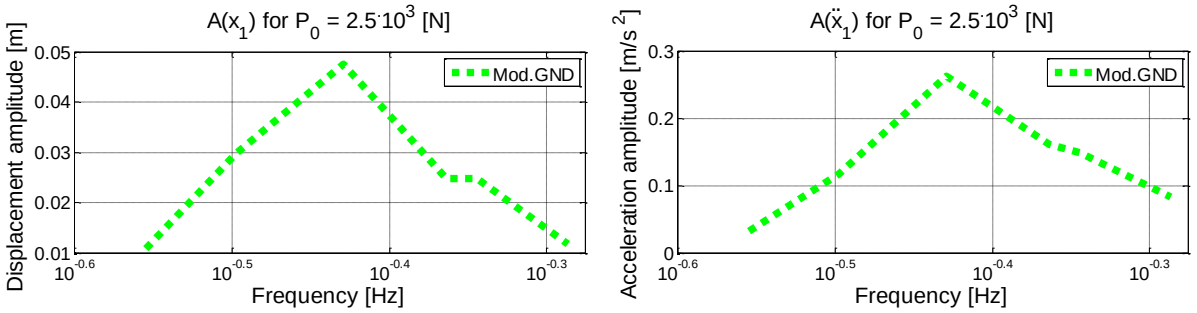

Figure 13. Tower tip displacement amplitude (left) and acceleration amplitude (right) output frequency response functions for baseline Vensys 82 model with MRTVA (see Table 1).

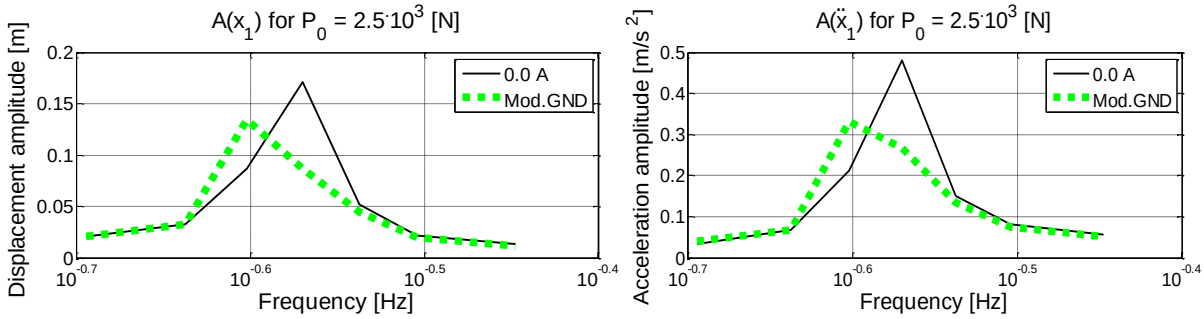

Figure 14. Tower tip displacement amplitude (left) and acceleration amplitude (right) output frequency response functions for modified Vensys 82 model with MRTVA (see Table 1).

Laboratory test rig

Laboratory test rig of wind turbine tower-nacelle system (Figure 15) was build according to the details specified in the *Wind turbine tower-nacelle model* section. It consists of vertically oriented titanium (Ti Gr.5) rod *1* (representing wind-turbine tower), and a set of steel plates *2* (representing nacelle and turbine assemblies) fixed to the top of the rod *1*, with MRTVA embedded. Titanium rod is rigidly mounted to the steel foundation frame *3*. MRTVA *4* is an additional mass moving horizontally along linear bearing guides, connected with the assembly representing nacelle via spring and Lord RD 1097-1 MR damper (Lord Rheonetic, 2002) in parallel. RD 1097-1 damper (which force depends on the current fed to its coil) is an actuator of such a vibration reduction system. MRTVA operates along the same direction as vibration excitation applied to the system. Force generated by vibration excitation system, i.e. The Modal Shop lightweight electrodynamic force exciter of 2060E series (TMS 2060E) (TMS, 2010) *5* with drive train assembly *6* of changeable leverage (enabling changeable force, displacement and velocity ranges) may be applied either to the rod *1* (modelling the tower, as in the picture) or to the set of steel plates *2* modelling nacelle/turbine. Excitation signal is generated by LDS Dactron *7* and amplified by TMS 2100E21-400 *8*.

Measurement and control system consists of laser vibrometer (x_1) with its controller *9*, laser displacement transducer (x_0) *10*, LVDT transducer ($x_1 - x_2$) *11*, tensometric stress transducers *12*, force (P_{MR}, among others) and acceleration transducers (not apparent in the picture) as well as transducers supply/conditioning system including MR damper signal amplifier *13*, and measuring-control PC *14* with MATLAB/Simulink/RT-CON applications (measured signals designations listed in brackets).

Selected test rig identification results are presented in the Table 2, while full identification problem is covered by author's separate publication.

Table 2. Selected parameters of laboratory test rig.

Length of the rod [10^{-3} m]	1507
Diameter of the rod [10^{-3} m]	70.5
Mass of the rod [kg]	26.06
Mass of the assembly located at the top (nacelle with TVA) [kg]	155.35

Figure 15. Laboratory test rig.

Laboratory test rig gives the possibility to model wind turbine tower vibration under various excitation sources. Moreover, the rig may be laid down on the horizontally excited platform to model vibration of buoy-floating wind turbine structures, or vibration due to seismic excitation. The above mentioned problems are described in detail in separate publications (Martynowicz, 2014a; Martynowicz and Szydło, 2014; Snamina et al., 2014).

Laboratory tests

Preliminary laboratory tests results are presented here. Initial analyses were conducted with relatively low excitation amplitudes to assure test facility safe operation. The first was excitation test with sine force of changing frequency (chirp). The force had horizontal direction, constant amplitude of 34.6 N and was applied to the rod (tower) midpoint (thus F_0 = 34.6 N). Figures 16 (a)(b) present time section of x_0 and x_1 displacement response within ca. (3.60, 4.30) Hz range for feedback system with modified ground-hook (*Mod.GND*) control algorithm in comparison with open-loop system (with 0.0A MR damper input current) exhibiting lowest x_0 and x_1 displacement amplitudes. The range of (3.60, 4.30) Hz comprises 1st tower bending mode of vibration, occurring for the system with MRTVA 'locked' (by input current of 0.6 A) at frequency of 3.82 Hz, that is ca. 0.2 Hz lower than frequency predicted by Comsol Multiphysics analyses. Such a relation between frequencies was predictable as FEM method imposes the additional stiffness on the model, while mass of test rig nacelle with MRTVA is slightly higher than nacelle mass assumed for FEM model (see Tables 2 and 3). Some differences in tower theoretical and laboratory model parameters are present, too. The maximum displacements amplitudes $max(A(x_1))$, $max(A(x_0))$ and their ratio: $max(A(x_1))/max(A(x_0))$ as well as maximum MR damper force values for MRTVA system operating in open-loop and feedback modes are all collected in the Table 3.

It is worth to note that MRTVA operating in feedback mode is by a small margin the most effective in tower deflection x_0 and x_1 reduction (Table 3, Figures 16) and simultaneously (thanks to displacements amplitudes minimisation) generates lowest value of maximum MR damper force. Maximum displacements amplitudes ratio values (resulting from the vibration mode shape) variation is insignificant for selected MR damper input current values, however it displays some system nonlinearities.

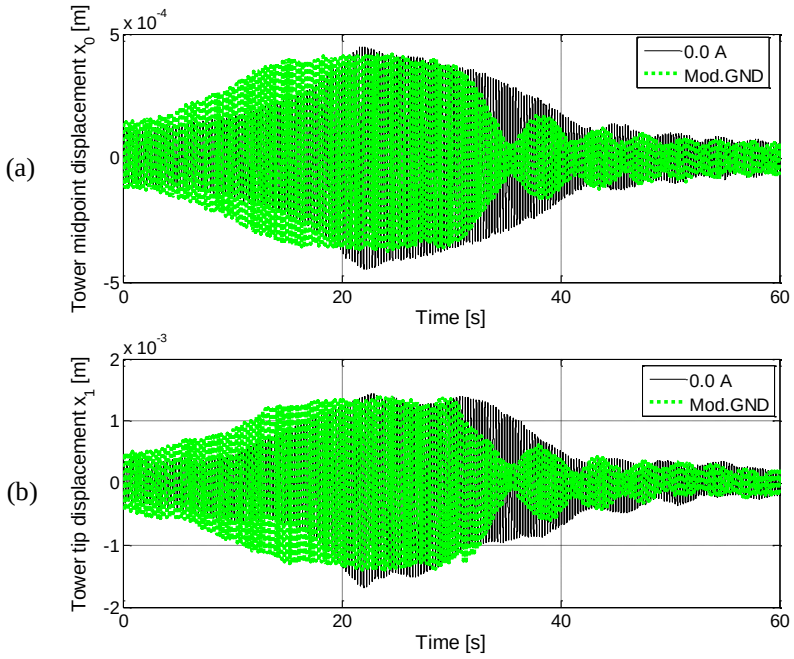

Figure 16. Responses of tower-nacelle system under chirp-type excitation

Table 3. Results of chirp-type excitation laboratory tests.

Configuration Details	Open-loop mode				Feedback mode
	0.00 A	***0.05 A***	***0.10 A***	***0.20 A***	***Mod.GND*** (Figures 16)
Max displ. ampl. $max(A(w_0))$ [10^{-3} m]	0.45	0.47	0.59	0.83	0.39
Max displ. ampl. $max(A(w_1))$ [10^{-3} m]	1.54	1.67	1.99	2.89	1.38
$max(A(w_1)) / max(A(w_0))$	3.46	3.53	3.40	3.50	3.51
Max MR Damper Force [N]	3.00	3.19	4.78	8.87	2.78

On a ground of these results, frequency characteristics were evaluated. Figures 17 (a)(b) present A(x_0) and A(x_1) output frequency response functions determined at F_0 = 30.5 N excitation within (3, 40) Hz frequency range for the open-loop system with 0.0 A and 0.1 A input currents, 0.6 A input current (i.e. MRTVA in 'locked' state), and feedback system with *Mod.GND* algorithm. These characteristics as well as x_0 and x_1 displacement amplitude values from the Table 3 indicate system is more damped than simulation model (details in author's separate paper on test rig identification). The typical for TVA two maxima cannot be observed in Figures 17 for 0.0 A as for simulation model. All of that causes control results to be compromised as lowest control signal value of 0.0 A is simultaneously the input current providing the best vibration reduction results from among all open-loop solutions with constant input current (Table 3, Figures 17) in relatively low force excitation conditions.

Following the above results and conclusions, the next test was undergone with significantly higher excitation amplitude, within the most interesting 1st bending resonance neighbourhood range. Figures 18 (a)(b) present A(x_0) and A(x_1) output frequency response functions determined at F_0 = 150 N, (3.25, 5.00) Hz excitation conditions for the open-loop system with 0.0 A input current and feedback system with *Mod.GND* algorithm. As can be inferred from Figures 18 (in comparison with Figures 17), MR damper pre-yield force is less dominant at relatively high excitation amplitudes, thus some control possibilities are there in comparison with *0.0 A* open-loop system, for which also the two local maxima are apparent as for the system with standard passive TVA.

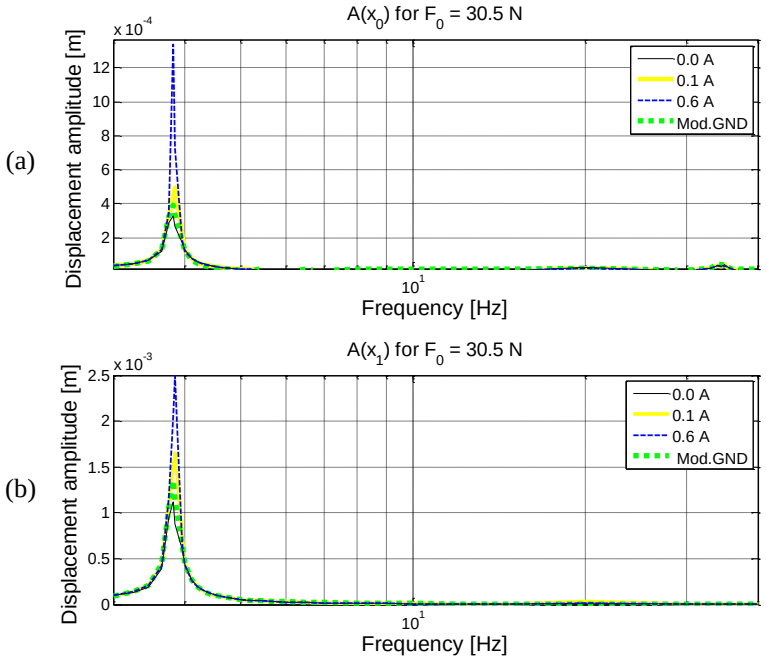

Figure 17. Tower midpoint displacement amplitude A(x_0) and tower tip displacement amplitude A(x_1) output frequency response functions

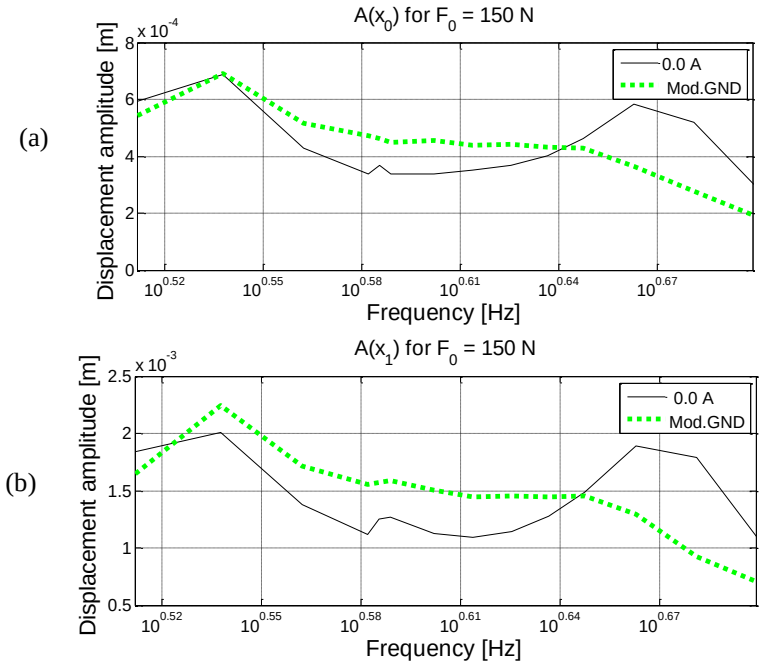

Figure 18. Tower midpoint displacement amplitude A(x_0) and tower tip displacement amplitude A(x_1) output frequency response functions

To more completely cope with the problem of too much MRTVA damping, test rig was reconfigured by increasing nacelle and absorber masses as well as stiffness of TVA spring, thus increasing damping ratio (and so MR damper input current) required for optimum (Den Hartog, 1985) TVA operation, while maintaining x_1 and x_2 displacements ranges (the laboratory test rig was designed in such a way that masses of the nacelle / absorber as well as spring stiffness may be changed, while MR damper type change is not considered due to limited market availability). The preliminary results obtained for the reconfigured system are presented in Figures 19 (a)(b). As can be observed, *Mod.GND* system delivers the most favourable response over the regarded (2.72, 4.72) Hz frequency range, as compared with the passive system with 0.0 A and 0.1 A control currents.

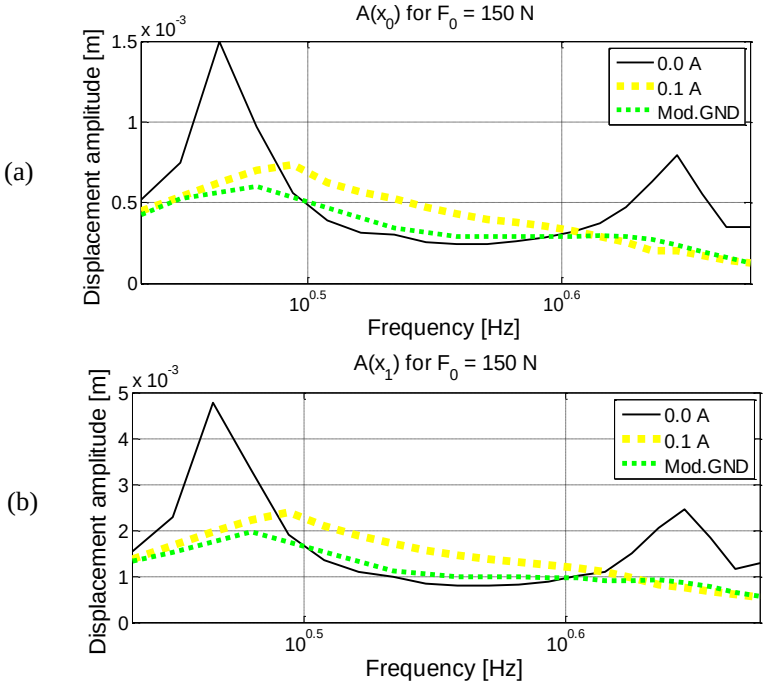

Figure 19. Tower midpoint displacement amplitude A(x_0) and tower tip displacement amplitude A(x_1) output frequency response functions (after reconfiguration)

Conclusion

The conducted comprehensive simulation study delivers a lot of valuable data concerning vibration reduction of tower-nacelle model with MRTVA. Vibration control results for the system equipped with MRTVA are improved in relation with the system that emulates standard TVA with linear (viscous) damper. Comsol/Simulink co-simulation tool is a good solution for control algorithms analysis, prototyping and implementation for continuous and continuous-discrete systems, however computational time is quite a problem.

The results of simulation analyses along with calculations concerning dynamic similarity of the proposed model with Vensys 82 real-world wind turbine (Snamina and Martynowicz, 2014; Snamina et al., 2014) served for estimation of the benefits of implementation of MRTVA for a full-scale structure. These include possible reduction of structure overall mass, significant reduction of tower deflection (thus bending fatigue) and nacelle acceleration amplitudes as well as possible operation at higher RPM to increase power production and decrease cost of energy factor, while reducing risk of structure failure due to wind, waves or earthquake induced vibration. The cost analysis however is nor subject of current research project.

Previous section results proved the laboratory test rig was more damped than simulation model and that compromised control possibilities as minimum control signal for feedback system (0.0 A) was providing the best vibration reduction results in open-loop case for low excitation amplitudes (F_0 = 30.5 N and F_0 = 34.6 N). To cope with that problem, excitation amplitude was increased (F_0 = 150 N) and test rig was reconfigured. Some preliminary laboratory-based validation results of new laboratory validation tests are presented here, while their full scope is covered by the separate papers (Martynowicz, 2015; Rosół and Martynowicz, 2015).

Further work program includes wide cooperation on implementation of such designed MRTVA system in the full scale structure within the scope of EU project.

Acknowledgment

This work was financed by the Polish National Science Centre project no. 2286/B/T02/2011/40.

References

Bak C, Bitsche R, Yde A, Kim T, Hansen MH, Zahle F, Gaunaa M, Blasques J, Dossing M, Wedel-Heinen JJ and Behrens T (2012) Light Rotor: The 10-MW reference wind turbine. In: *European Wind Energy Association Annual Event*, 16–19.04.2012, Copenhagen, Denmark.

Butt UA and Ishihara T (2012) Seismic Load Evaluation of Wind Turbine Support Structures Considering Low Structural Damping and Soil Structure Interaction. In: *European Wind Energy Association Annual Event*, 16–19.04.2012, Copenhagen, Denmark.

Den Hartog JP (1985) *Mechanical Vibrations*. Mineola: Dover Publications.

Enevoldsen I and Mork KJ (1996) Effects of Vibration Mass Damper in a Wind Turbine Tower. *Mech. Struct. & Mach.*, 24(2): 155–187.

Hansen MH, Fuglsang P, Thomsen K and Knudsen T (2012) Two Methods for Estimating Aeroelastic Damping of Operational Wind Turbine Modes from Experiments. In: *European Wind Energy Association Annual Event*, 16–19.04.2012, Copenhagen, Denmark.

Jain P (2011) *Wind Energy Engineering*. McGRAW-HILL.

Jelavić M, Perić N and Petrović I (2007) Damping of Wind Turbine Tower Oscillations through Rotor Speed Control. In: *International Conference on Ecologic Vehicles & Renewable Energies*, March 29–April 1, 2007, Monaco.

Kciuk S and Martynowicz P (2011) Special application magnetorheological valve numerical and experimental analysis. *Control engineering in materials processing, Diffusion and Defect Data – Solid State Data, Pt. B, Solid State Phenomena*, Vol. 177: 102–115.

Kirkegaard PH, Nielsen SRK, Poulsen BL, Andersen J, Pedersen LH and Pedersen BJ (2002) Semiactive vibration control of a wind turbine tower using an MR damper. In: Grundmann H and Schueller GI (eds) *Struct. Dynamics EURODYN*. Lisse: Swets & Zeitlinger.

Koo JH and Ahmadian M (2007) Qualitative Analysis of Magneto-Rheological Tuned Vibration Absorbers: Experimental Approach. *Journal of Intelligent Material Systems and Structures*, Vol. 18, December 2007.
Laalej H, Lang ZQ, Sapinski B and Martynowicz P (2012) MR damper based implementation of nonlinear damping for a pitch plane suspension system. *Smart Materials and Structures*, Vol. 21.
Lord Rheonetic (2002) MR Controllable Friction Damper RD-1097-01. Product Bulletin.
Łatas W and Martynowicz P (2012) Modelowanie drgań układu maszt-gondola elektrowni wiatrowej z tłumikiem dynamicznym. *Modelowanie Inżynierskie*, nr 44, t. 13: 187–198.
Martynowicz P (2014a) Development of Laboratory Model of Wind Turbine's Tower-Nacelle System with Magnetorheological Tuned Vibration Absorber. *Solid State Phenomena*, Vol. 208: 40–51.
Martynowicz P (2014b) Wind turbine's tower-nacelle model with magnetorheological tuned vibration absorber – numerical and experimental analysis. In: *6WCSCM*: *Sixth World Conference on Structural Control and Monitoring – proceedings of the 6th edition of the World conference of the International Association for Structural Control and Monitoring (IACSM)*, Barcelona, Spain, 15–17 July 2014.
Martynowicz P (2015) Study of vibration control using laboratory test rig of wind turbine's tower-nacelle system with MR damper based tuned vibration absorber. *Bulletin of the Polish Academy of Sciences Technical Sciences* (in review).
Martynowicz P and Szydło Z (2013) Wind turbine's tower-nacelle model with magnetorheological tuned vibration absorber: the laboratory test rig. In: *Proceedings of the 14th International Carpathian Control Conference (ICCC)*, Rytro, Poland, May 26–29, 2013.
Maślanka M, Sapiński B and Snamina J (2007) Experimental Study of Vibration Control of a Cable With an Attached MR Damper. *Journal of Theoretical and Applied Mechanics* 45, 4: 893–917, Warsaw.
Matachowski F and Martynowicz P (2012) Analiza dynamiki konstrukcji elektrowni wiatrowej z wykorzystaniem środowiska Comsol Multiphysics. *Modelowanie Inżynierskie*, nr 44, t. 13: 209–216.
Namik H and Stol K (2011) Performance analysis of individual blade pitch control of offshore wind turbines on two floating platforms. *Mechatronics* 21: 691–703.
Neelakantan VA and Washington GN (2008) Vibration Control of Structural Systems using MR dampers and a 'Modified' Sliding Mode Control Technique. *Journal of Intelligent Material Systems and Structures*, Vol. 19.
Oh S and Ishihara T (2013) A Study on Structure Parameters of an Offshore Wind Turbine by Excitation test Using Active Mass Damper. In: *EWEA Offshore*, 19-21.11.2013, Frankfurt.
Rosół M and Martynowicz P (2015) Identification of Laboratory Model of Wind Turbine's Tower-Nacelle System with MR Damper Based Tuned Vibration Absorber. *Mechanical Systems and Signal Processing* (in review).
Rotea MA, Lackner MA and Saheba R (2010) Active Structural Control of Offshore Wind turbines. In: *48th AIAA Aerospace Sciences Meeting Including the New Horizons Forum and Aerospace Exposition*, 4–7 January 2010, Orlando, Florida.
Sapiński B (2008) *Real-time control of magnetorheological dampers in mechanical systems*. Cracow: AGH University of Science and Technology Press.
Sapiński B and Rosół M (2008) Autonomous control system for a 3 DOF pitch-plane suspension system with MR shock absorbers. *Computers and Structures*, 86: 379–385.
Sapiński B (2011) Experimental study of a self-powered and sensing MR damper-based vibration control system. *Smart Materials and Structures*, 20, 105007.
Shan W and Shan M (2012) Gain Scheduling Pitch Control Design for Active Tower Damping and 3p Harmonic Reduction. In: *European Wind Energy Association Annual Event*, 16–19.04.2012, Copenhagen, Denmark.
Shen YJ, Wang L, Yang SP and Gao GS (2013) Nonlinear dynamical analysis and parameters optimization of four semi-active on-off dynamic vibration absorbers. *Journal of Vibration and Control*, January 2013, vol. 19, no. 1: 143–160.
Snamina J, Martynowicz P and Łatas W (2014) Dynamic similarity of wind turbine's tower-nacelle system and its scaled model. *Solid State Phenomena*, Vol. 208: 29–39.
Snamina J and Martynowicz P (2014) Prediction of characteristics of wind turbine's tower-nacelle system from investigation of its scaled model. In: *6WCSCM*: *Sixth World Conference on Structural*

Control and Monitoring – proceedings of the 6th edition of the World conference of the International Association for Structural Control and Monitoring (IACSM), Barcelona, Spain, 15–17 July 2014.
TMS (2010) 60 Lbf Modal Shaker. The Modal Shop Inc.
Tsouroukdissian A, Carcangiu CE, Pineda Amo I, Martin M, Fischer T, Kuhnle B and Scheu M (2011) Wind Turbine Tower Load Reduction using Passive and Semiactive Dampers. *European Wind Energy Association Annual Event*, Brussels.